Japanese Journal of Radiology (2019) 37:399–411
https://doi.org/10.1007/s11604-019-00823-5

ORIGINAL ARTICLE

Effects of acquisition method and reconstruction algorithm for CT number measurement on standard-dose CT and reduced-dose CT: a QIBA phantom study

Yoshiharu Ohno[1,2] · Yasuko Fujisawa[3] · Kenji Fujii[3] · Naoki Sugihara[3] · Yuji Kishida[4] · Shinichiro Seki[1,2] · Takeshi Yoshikawa[1,2]

Received: 27 December 2018 / Accepted: 17 February 2019 / Published online: 25 February 2019

Abstract

Purpose To compare the effect of different acquisition and reconstruction methods on the radiation dose and accuracy of CT number measurements, using a 320-detector row CT and a Quantitative Imaging Biomarker Alliance (QIBA) recommended phantom.

Materials and methods Acquisitions were performed on a 320-detector row CT, as 64- and 80-detector row helical and wide detector step-and-shoot (i.e., wide volume) acquisitions with tube currents of 400 mA, 100 mA, 50 mA, 20 mA, and 10 mA. Image was reconstructed with the filtered back projection (FBP), adaptive iterative dose reduction using 3D processing (AIDR 3D), and forward projected model-based iterative reconstruction (FIRST) methods. The difference between measured CT numbers and the actual -856HU value of the phantom insert was determined by each CT acquisition protocol. Differences in actual and measured CT numbers were compared among acquisitions and among reconstruction methods by means of Tukey's HSD test.

Results The CT number obtained with 64-detector row helical acquisition was significantly larger than that obtained with others ($p < 0.0001$). At each tube current, the CT number reconstructed with FIRST was significantly smaller than that with others ($p < 0.0001$).

Conclusion Acquisition and reconstruction methods are significantly affecting radiation dose reduction and accuracy of CT number measurements on a phantom study.

Keywords Lung · CT · Radiation dose · Reconstruction algorithm · Scanning method

Introduction

Computed tomography (CT) has been suggested as useful for management of chronic obstructive pulmonary disease (COPD). It can be used for COPD phenotyping and for early detection of emphysema in smokers, based on lung density measurement as an imaging biomarker [1–4]. Quantitatively assessed CT lung density metrics are typically evaluated as the percentage of voxels with CT numbers below a given threshold, or as a single CT number below a set relative lung volume, the relative area below − 950 Hounsfield units (HU) (RA_{950}), 15th percentile density (PD15), etc. Therefore, reduction of variability in the density metrics has been considered an important factor in chest CT examination [5–8].

Since 2007, CT density variability has been investigated and efforts to reduce it have been organized by a few academic societies such as the Quantitative Imaging Biomarker

✉ Yoshiharu Ohno
yosirad@kobe-u.ac.jp; yosirad@med.kobe-u.ac.jp; yoshiharuohno@aol.com

1 Division of Functional and Diagnostic Imaging Research, Department of Radiology, Kobe University Graduate School of Medicine, 7-5-2 Kusunoki-cho, Chuo-ku, Kobe, Hyogo 650-0017, Japan

2 Advanced Biomedical Imaging Research Center, Kobe University Graduate School of Medicine, Kobe, Hyogo, Japan

3 Canon Medical Systems Corporation, Otawara, Tochigi, Japan

4 Division of Radiology, Department of Radiology, Kobe University Graduate School of Medicine, Kobe, Hyogo, Japan

Alliance (QIBA) of the Radiological Society of North America, the European Imaging Biomarker Alliance (EIBALL) of the European Society of Radiology and Japan QIBA of the Japanese Society of Radiology. In addition, QIBA has summarized the longitudinal studies in terms of repeatability by performing meta-analysis of the published data [9–14] and reported them as a QIBA profile [15, 16]. For reducing the variance of CT number measurement, QIBA has published the data of the COPDGene I or II phantom (Phantom Labs, Salem, NY, USA) examinations by four major CT vendors together with best-effort matching protocols for a variety of tube potentials and exposure settings [17, 18]. However, these studies [17, 18] have not dealt the different acquisition methods such as helical acquisition and wide-volume acquisition (i.e., step-and-shoot acquisition) on 320- and 256-detector row CTs provided by Canon Medical Systems Corporation and General Electronic Healthcare, as well as the different reconstruction algorithms such as filtered back projection (FBP) and hybrid-type or model-based iterative reconstruction (IR) methods.

We hypothesized that the wide-volume acquisition or IR methods could more accurately evaluate lung CT number than helical acquisition or FBP method at different radiation dose settings at the QIBA suggested phantom study. The purpose of this study was thus to directly compare lung CT number measurement accuracy between wide-volume and helical acquisitions and among hybrid-type and model-based IR and FBP methods on a 320-detector row CT at different radiation dose setting in a QIBA recommended phantom study.

Materials and methods

Protocol, support, and funding

This study was financially and technically supported by Canon Medical Systems Corporation. Three of the authors (Y.F, K.F, and N.S) are employees of Canon Medical Systems, but did not have control over any of the data used in this study.

Phantom

The COPDGene II phantom (Phantom Labs) consists of three reference foam inserts (labeled 4 lb, 12 lb, and 20 lb, corresponding to nominal densities of 64.2 kg/m^3, 192.6 kg/m^3, and 321.0 kg/m^3, respectively), as well as air and water samples, embedded in a larger oval lung density equivalent foam made of a specially formulated urethane, with a CT number of − 856 HU, and attenuated by a chest wall equivalent ring (Fig. 1) [18–20]. The water equivalent diameter of the phantom (Dw) was determined as 296 mm. In addition, all gold standards of foam inserts in this study were provided from Phantom Labs.

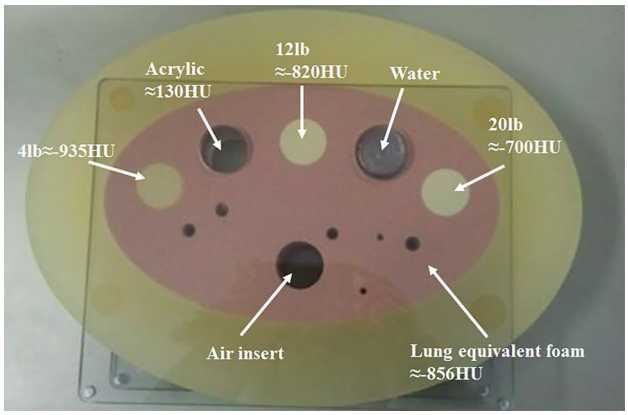

Fig. 1 Commercially available QIBA recommended phantom "COPDGene II" provided by Phantom Laboratory and used in this study. Photograph of commercially available QIBA recommended phantom, "COPDGene II" (Phantom Laboratory), used in this study. The CT numbers obtained with a typical 120 kV scan are approximate

CT examinations

All CT data were obtained with a 320-detector row CT (Aquilion ONE; Canon Medical Systems Corporation, Otawara, Tochigi, Japan) by means of wide-volume (i.e. step-and-shoot acquisition) and helical acquisitions setting 64- and 80-detectors. For each acquisition, the following scan parameters were used: 120 kVp, 0.5 s gantry rotation time, 512 × 512 matrix, and 400 mm field of view. In addition, the tube currents used in this study were 400 mA as standard-dose CT (standard-dose CT at 400 mA: 400 mA-CT), 100 mA (reduced-dose CT at 100 mA: 100 mA-CT), 50 mA (reduced-dose CT at 50 mA: 50 mA-CT), 20 mA (reduced-dose CT at 20 mA: 20 mA-CT), and 10 mA (reduced-dose CT at 10 mA: 10 mA-CT). A detector collimation of 320 × 0.5 mm and a step-and-shoot acquisition were used for each wide-volume scan, a 64 × 0.5 mm detector collimation and a beam pitch of 0.83 for each 64-detector row helical acquisition, and an 80 × 0.5 mm detector collimation and a beam pitch of 0.81 for each 80-detector helical acquisition. Detail of radiation dose on each CT protocol is shown in Table 1.

For each CT protocol acquisition, the phantom was scanned three times at each tube current, and thin-section CT images obtained at all tube currents were reconstructed at a contiguous section thickness of 1 mm with the FBP, adaptive iterative dose reduction system using a three-dimensional processing (AIDR 3D: Canon Medical) and forward projected model-based iterative reconstruction (FIRST: Canon Medical) methods. AIDR 3D and FIRST were used as the

Table 1 Radiation dose of each CT protocol

CT protocol	Acquisition method	CTDIvol (mGy)	SSDE (mGy)
400 mA-CT	64-Detector row helical acquisition	29	36.3
	80-Detector row helical acquisition	26.6	33.3
	Wide-volume acquisition	22.7	28.4
100 mA-CT	64-Detector row helical acquisition	7	8.8
	80-Detector row helical acquisition	6.3	7.9
	Wide-volume acquisition	5.4	6.8
50 mA-CT	64-Detector row helical acquisition	3.5	4.4
	80-Detector row helical acquisition	3.2	4.0
	Wide-volume acquisition	2.7	3.4
20 mA-CT	64-Detector row helical acquisition	1.4	1.8
	80-Detector row helical acquisition	1.3	1.6
	Wide-volume acquisition	1.1	1.4
10 mA-CT	64-Detector row helical acquisition	0.7	0.9
	80-Detector row helical acquisition	0.6	0.8
	Wide-volume acquisition	0.5	0.6

CTDIvol volume computed tomography dose index, *SSDE* size-specific dose estimation

hybrid-type and model-based iterative reconstruction techniques for this study. In addition, the FBP and AIDR 3D methods were applied for the reconstruction lung kernel (FC17, Canon Medical).

Image analysis

Each phantom density was determined as a value averaged from region-of-interest (ROI) measurements, which were performed ten times by a radiologist with 24 years' experience (Y.O) using a commercially available workstation (Vitrea; Vital Images, Inc., Minnesota, MN, USA). On each CT protocol, ROI placement was performed at three slices as follows: 3 cm prior to center slice, center slice of QIBA phantom, and 3 cm posterior to center slice. Therefore, total 630 ROIs (7 ROIs placed at all density phantoms × 3 slices × 3 scan × 10 times = 630 ROIs) measurements were performed in this study.

Statistical analysis

Pearson's correlation analyses were performed to determine the relationship of actual and measured CT numbers for each phantom using each protocol.

For assessing repeatability for each CT number measurement in the lung density phantom, repeatability coefficient of each CT acquisition was evaluated by Bland–Altman's method [20].

To assess the effect of a given scanning method, reconstruction algorithm and tube current used for evaluating a CT number in the lung density phantom, the CT number measured within the lung phantom was compared with the gold standard by means of ANOVA followed by Dunnett's test. Moreover, Pearson's correlation analyses were performed to determine the relationship of actual and measured CT numbers for each phantom using each protocol.

To evaluate the effect of a given acquisition method for CT number assessment with the same reconstruction algorithm, differences between actual and measured CT numbers obtained with the lung density phantom were compared or 64-detector row helical acquisition, 80-detector row helical acquisition, and wide-volume acquisition methods at each tube current by means of ANOVA followed by Tukey's HSD test.

To assess the effect of a given reconstruction algorithm on CT number assessment for the same scanning method, differences between actual and measured CT numbers obtained with the lung density phantom were also compared for FBP, AIDR 3D, and FIRST at each tube current by means of ANOVA followed by Tukey's HSD test.

Finally, the limits of agreement between actual and measured CT numbers obtained with the lung density were assessed for each protocol by means of Bland–Altman's analyses [21, 22].

A p value < 0.05 was considered statistically significant for all statistical analyses.

Results

Phantom CT images obtained by means of 64-detector row helical scanning, 80-detector row helical acquisition, and wide-volume acquisition at each tube current and reconstructed with each of the three methods are shown in Figs. 2, 3, and 4.

On correlations between actual and measured CT numbers, there were significant and excellent correlations

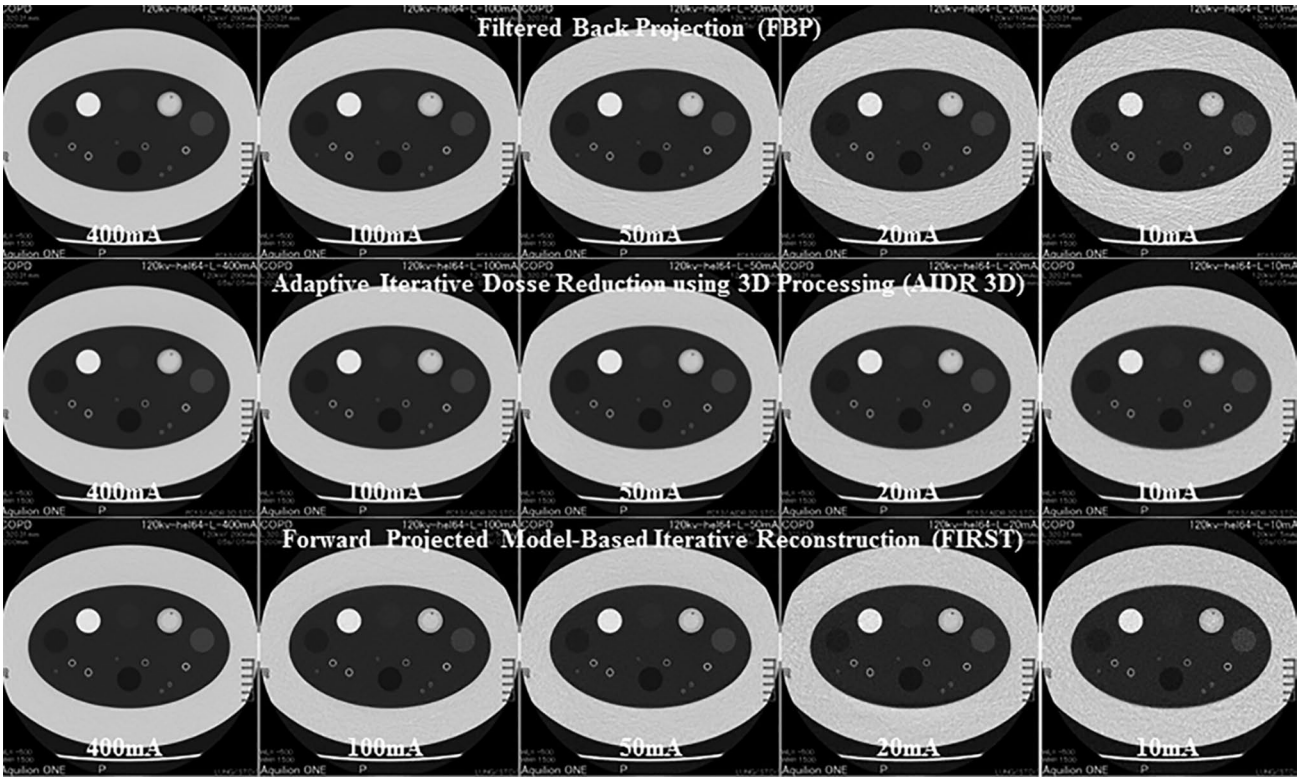

Fig. 2 CT images obtained by 64-detector row helical scan at 400 mA-CT, 100 mA-CT, 50 mA-CT, 20 mA-CT, and 10 mA-CT, and reconstructed with the FBP, AIDR 3D, and FIRST methods. Reduction in tube currents resulted in gradual increase in image noise on CT images reconstructed by the FBP method, and a smaller increase in those reconstructed by the AIDR 3D and FIRST methods

between actual and measured CT numbers for each protocol ($r = 0.99$, $p < 0.0001$).

Reproducibility of each CT protocol and results of comparisons of measured CT numbers in the lung density phantom with the corresponding gold standard for all protocols are shown in Table 2.

On 64-detector row helical acquisition, reproducibility coefficient (RC) of each CT protocol reconstructed by FBP method was as follows: 400 mA-CT, 0.0 ± 0.3HU; 100 mA-CT, 0.0 ± 0.3HU; 50 mA-CT, 0.0 ± 0.4HU; 20 mA-CT, 0.0 ± 0.5HU; 10 mA-CT, 0.0 ± 0.7HU. When reconstructed by AIDR 3D, RC of each CT protocol was determined as follows: 400 mA-CT, 0.0 ± 0.3HU; 100 mA-CT, 0.0 ± 0.3HU; 50 mA-CT, 0.0 ± 0.4HU; 20 mA-CT, 0.0 ± 0.4HU; 10 mA-CT, 0.0 ± 0.5HU. In addition, RC of each CT protocol reconstructed by FIRST was assessed as follows: 400 mA-CT, 0.0 ± 0.2HU; 100 mA-CT, 0.0 ± 0.2HU; 50 mA-CT, 0.0 ± 0.2HU; 20 mA-CT, 0.0 ± 0.3HU; 10 mA-CT, 0.0 ± 0.4HU.

When assessed 80-detector row helical acquisition, RC of each CT protocol reconstructed by the FBP method was as follows: 400 mA-CT, 0.0 ± 0.3HU; 100 mA-CT, 0.0 ± 0.3HU; 50 mA-CT, 0.0 ± 0.4HU; 20 mA-CT, 0.0±0.4HU; 10 mA-CT, 0.0 ± 0.6HU. For AIDR 3D, RC of each CT protocol was evaluated as follows: 400 mA-CT, 0.0 ± 0.3HU; 100 mA-CT, 0.0 ± 0.3HU; 50 mA-CT, 0.0 ± 0.3HU; 20 mA-CT, 0.0 ± 0.3HU; 10 mA-CT, 0.0 ± 0.5HU. In addition, RC of each CT protocol reconstructed by FIRST was determined as follows: 400 mA-CT, 0.0 ± 0.2HU; 100 mA-CT, 0.0 ± 0.2HU; 50 mA-CT, 0.0 ± 0.2HU; 20 mA-CT, 0.0 ± 0.2HU; 10 mA-CT, 0.0 ± 0.4HU.

On wide-volume acquisition, RC of each CT protocol reconstructed by FBP method was as follows: 400 mA-CT, 0.0 ± 0.2HU; 100 mA-CT, 0.0 ± 0.2HU; 50 mA-CT, 0.0 ± 0.3HU; 20 mA-CT, 0.0 ± 0.4HU; 10 mA-CT, 0.0 ± 0.6HU. When reconstructed by AIDR 3D, RC of each CT protocol was evaluated as follows: 400 mA-CT, 0.0 ± 0.2HU; 100 mA-CT, 0.0 ± 0.2HU; 50 mA-CT, 0.0 ± 0.3HU; 20 mA-CT, 0.0 ± 0.3HU; 10 mA-CT, 0.0 ± 0.4HU. In addition, RC of each CT protocol reconstructed by FIRST was determined as follows: 400 mA-CT, 0.0 ± 0.2HU; 100 mA-CT, 0.0 ± 0.2HU; 50 mA-CT, 0.0 ± 0.2HU; 20 mA-CT, 0.0 ± 0.2HU; 10 mA-CT, 0.0 ± 0.3HU.

With 64- and 80-detector row helical acquisition, mean measured CT numbers in the lung density phantom for each protocol showed significant differences with the

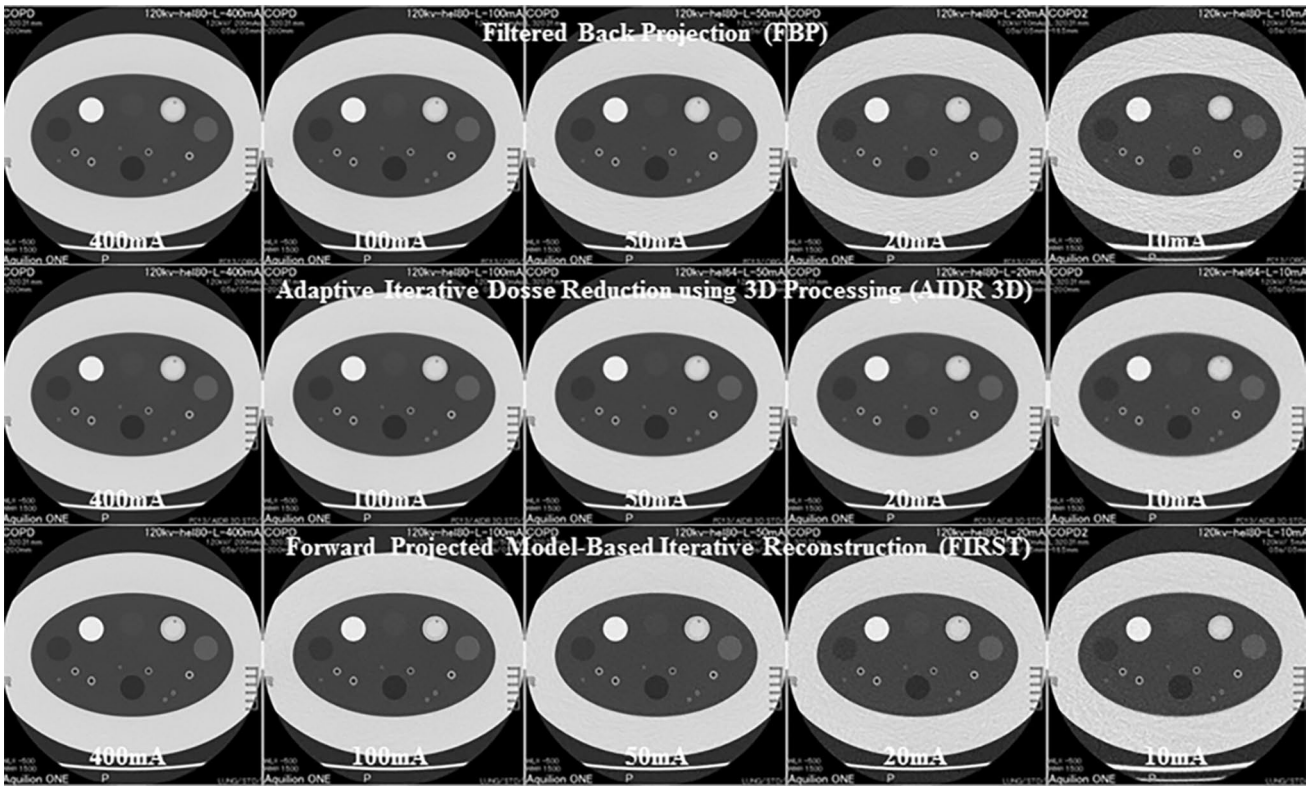

Fig. 3 CT images obtained by 80-detector row helical scan at 400 mA-CT, 100 mA-CT, 50 mA-CT, 20 mA-CT, and 10 mA-CT, and reconstructed with the FBP, AIDR 3D, and FIRST methods. Reduction in tube currents resulted in gradual increase in image noise on CT images reconstructed by the FBP method, and a smaller increase in those reconstructed with the AIDR 3D and FIRST methods

corresponding gold standard (both helical scans: $p < 0.0001$). With wide-volume acquisition, mean measured CT numbers in the lung density phantom obtained using all the protocols reconstructed with FBP ($p < 0.0001$) and AIDR 3D ($p < 0.0001$) and the protocol at 10 mA reconstructed with FIRST ($p = 0.03$) were significantly different those of the corresponding gold standard. Moreover, there were significant correlations between actual and measured CT numbers for each protocol ($r = 0.99$, $p < 0.0001$).

Results of a comparison between actual and measured CT numbers obtained with the three scan methods at the same tube current and with the same reconstruction method are shown in Table 3. At each tube current and for each reconstruction method, the CT number differences obtained with 64-detector row helical acquisition were significantly larger than their 80-detector row helical and wide-volume acquisition counterparts ($p < 0.0001$). In addition, 80-detector row helical acquisition CT number differences were significantly larger than their wide-volume acquisition counterparts ($p < 0.0001$).

Differences between actual and measured CT numbers among the three reconstruction methods with the same acquisition method and at the same tube current are shown in Table 4. For each acquisition at all tube currents, CT number differences for FIRST were significantly smaller than those for FBP and AIDR 3D ($p < 0.0001$). In addition, CT number differences for AIDR 3D were significantly smaller than those for FBP at all tube currents except 400 mA-CT ($p < 0.0001$).

The limits of agreement between actual and measured CT numbers in the lung density phantom for all CT protocols are shown in Table 5. A comparison of the limits of agreement for all scan methods and using each reconstruction algorithm showed that those values obtained with wide-volume acquisition were smaller than their 64- and 80-detector row helical acquisition counterparts at each tube current and with the same reconstruction methods. In addition, the 80-detector row helical acquisition values were lower than their 64-detector row helical acquisition counterparts at each tube current and with the same reconstruction methods. A comparison of the limits of agreement for all reconstruction methods showed that those values of AIDR 3D and FIRST were smaller than those of FBP at each tube current and using the same acquisition. In addition, the values for FIRST were lower than those for AIDR 3D at each tube current and with the same acquisition.

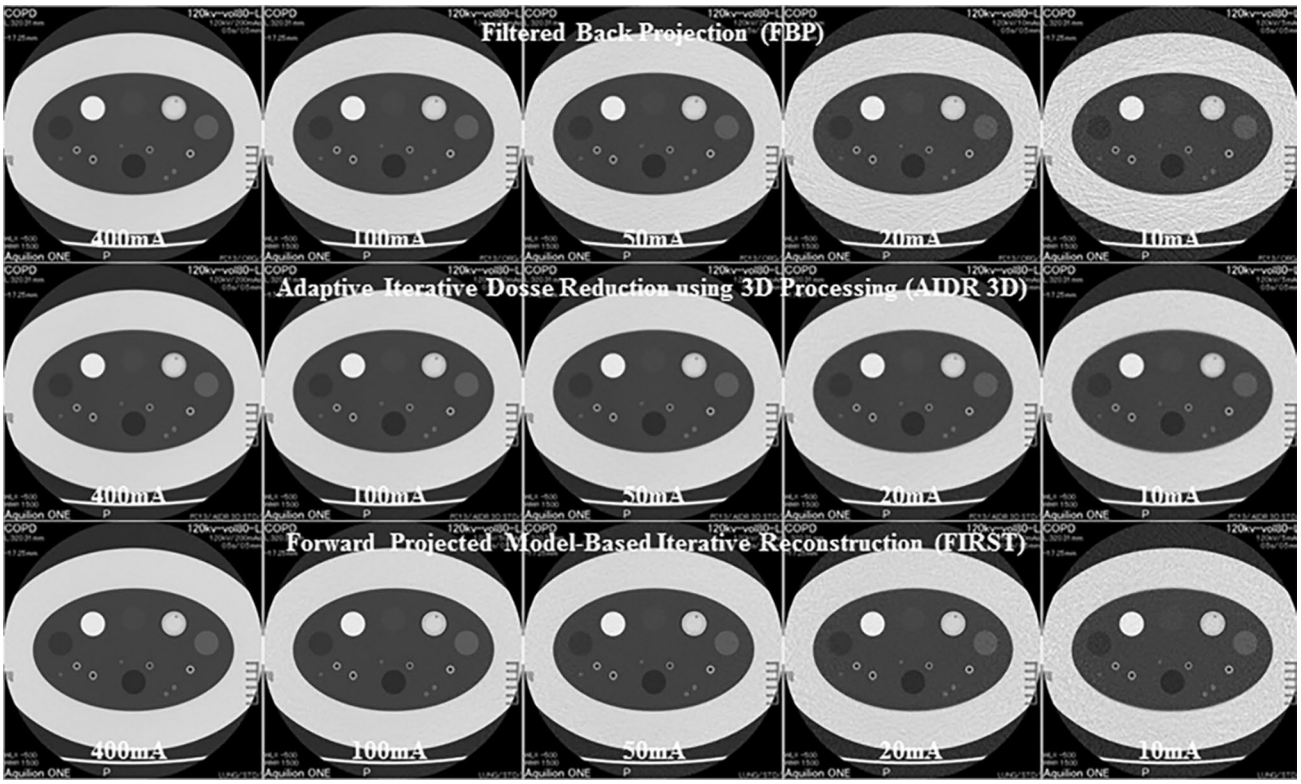

Fig. 4 CT images obtained by wide-volume scanning at 400 mA-CT, 100 mA-CT, 50 mA-CT, 20 mA-CT, and 10 mA-CT, and reconstructed with the FBP, AIDR 3D, and FIRST methods. Reduction in tube currents resulted in gradual increase in image noise on CT images reconstructed by the FBP method and a smaller increase in those reconstructed with the AIDR 3D and FIRST methods

Discussion

Our results show that both acquisition and reconstruction methods significantly affect accuracy of CT number assessment for lung in a QIBA recommended phantom study. In addition, the wide-volume scan and the FIRST methods suggest to be potentially better for radiation dose reduction while maintaining the accuracy of CT number assessment for lung than other scan and reconstruction methods. To the best of our knowledge, no other studies have assessed the capabilities of these methods for accurate CT number measurement and radiation dose reduction using ADCT in this setting, because QIBA study was mainly focused on standard helical acquisition on 64-detector row CT at standard tube current in each vendor and reconstructed by the FBP method. In addition, QIBA had not been assessed CT number measurement by 64- and 80-detector row helical acquisition as well as wide-volume acquisition and reconstructed by on not only FBP, but also IR methods. Therefore, ADCT, which has the capability for obtaining CT data by each acquisition method as well as all reconstruction methods, might be useful for assessing for this study purposes.

When assessed reproducibility coefficient for CT number measurement on the lung density phantom by all CT protocols, all reproducibility coefficients were equal to or less than 0.7 HU and considered as small enough for clinical purpose.

Assessment of the effect of acquisition method, reconstruction algorithm and tube current on evaluating CT numbers in the lung density phantom and mean measured CT numbers in the lung density phantom for each protocol using 64- and 80-detector row helical acquisition and all reconstruction methods showed that these numbers differed significantly from those of the gold standard. On the other hand, when wide-volume acquisition was used, mean measured CT numbers on CT images reconstructed with the FIRST method at all tube currents except 10 mA showed no significant differences. Therefore, wide-volume acquisition as well as the FIRST method would be better than helical acquisitions for accurate lung density measurement based on the results obtained with the QIBA recommended phantom study.

Examination of the relationship between actual and measured CT numbers in different forms obtained with all CT protocols within the QIBA recommended phantom showed significant and excellent correlations between not only 400 mA-CT with 64-detector row helical acquisition and the FBP method, which are considered the standard protocol for

Table 2 Reproducibility coefficient of CT numbers measured in lung density phantom on each protocol and result of comparison of CT numbers measured in lung density phantom on each protocol with gold standard

Acquisition method	Reconstruction method	CT protocol	Reproducibility coefficient (HU) (Mean ± standard deviation)	CT number (HU) (Mean ± standard deviation)
64-Detector row helical acquisition	FBP	400 mA-CT	0.0 ± 0.3	− 861.3 ± 0.2*
		100 mA-CT	0.0 ± 0.3	− 861.9 ± 0.2*
		50 mA-CT	0.0 ± 0.4	− 862.4 ± 0.3*
		20 mA-CT	0.0 ± 0.5	− 865.8 ± 0.3*
		10 mA-CT	0.0 ± 0.7	− 870.0 ± 0.5*
	AIDR 3D	400 mA-CT	0.0 ± 0.3	− 861.3 ± 0.2*
		100 mA-CT	0.0 ± 0.3	− 861.5 ± 0.2*
		50 mA-CT	0.0 ± 0.4	− 861.4 ± 0.2*
		20 mA-CT	0.0 ± 0.4	− 861.7 ± 0.2*
		10 mA-CT	0.0 ± 0.5	− 862.3 ± 0.5*
	FIRST	400 mA-CT	0.0 ± 0.2	− 858.2 ± 0.2*
		100 mA-CT	0.0 ± 0.2	− 858.4 ± 0.4*
		50 mA-CT	0.0 ± 0.2	− 858.5 ± 0.5*
		20 mA-CT	0.0 ± 0.3	− 859.1 ± 0.4*
		10 mA-CT	0.0 ± 0.4	− 859.6 ± 0.6*
80-Detector row helical acquisition	FBP	400 mA-CT	0.0 ± 0.3	− 858.9 ± 0.2*
		100 mA-CT	0.0 ± 0.3	− 859.6 ± 0.1*
		50 mA-CT	0.0 ± 0.4	− 860.3 ± 0.2*
		20 mA-CT	0.0 ± 0.4	− 862.4 ± 0.3*
		10 mA-CT	0.0 ± 0.6	− 868.6 ± 0.5*
	AIDR 3D	400 mA-CT	0.0 ± 0.3	− 858.9 ± 0.1*
		100 mA-CT	0.0 ± 0.3	− 859.2 ± 0.1*
		50 mA-CT	0.0 ± 0.3	− 859.2 ± 0.1*
		20 mA-CT	0.0 ± 0.3	− 859.4 ± 0.2*
		10 mA-CT	0.0 ± 0.5	− 860.2 ± 0.4*
	FIRST	400 mA-CT	0.0 ± 0.2	− 857.5 ± 0.1*
		100 mA-CT	0.0 ± 0.2	− 856.8 ± 0.2*
		50 mA-CT	0.0 ± 0.2	− 856.8 ± 0.5*
		20 mA-CT	0.0 ± 0.2	− 857.0 ± 0.4*
		10 mA-CT	0.0 ± 0.4	− 857.7 ± 0.5*
Wide-volume acquisition	FBP	400 mA-CT	0.0 ± 0.2	− 857.8 ± 0.2*
		100 mA-CT	0.0 ± 0.2	− 858.4 ± 0.2*
		50 mA-CT	0.0 ± 0.3	− 859.0 ± 0.3*
		20 mA-CT	0.0 ± 0.4	− 861.5 ± 0.4*
		10 mA-CT	0.0 ± 0.6	− 867.0 ± 0.6*
	AIDR 3D	400 mA-CT	0.0 ± 0.2	− 857.8 ± 0.2*
		100 mA-CT	0.0 ± 0.2	− 858.0 ± 0.2*
		50 mA-CT	0.0 ± 0.3	− 858.0 ± 0.3*
		20 mA-CT	0.0 ± 0.3	− 858.4 ± 0.3*
		10 mA-CT	0.0 ± 0.4	− 859.0 ± 0.4*
	FIRST	400 mA-CT	0.0 ± 0.2	− 856.2 ± 0.3
		100 mA-CT	0.0 ± 0.2	− 855.8 ± 0.4
		50 mA-CT	0.0 ± 0.2	− 855.7 ± 0.5
		20 mA-CT	0.0 ± 0.2	− 855.6 ± 0.5
		10 mA-CT	0.0 ± 0.3	− 856.5 ± 0.5**

FBP filtered back projection, *AIDR 3D* adaptive iterative dose reduction using 3D processing, *FIRST* forward projected model-based iterative reconstruction

*Significant difference with gold standard ($p < 0.0001$)

**Significant difference with gold standard ($p = 0.03$)

lung density measurement [19, 23–28], but also in the case of other protocols. Some of these findings were compatible with those reported in the literature [19, 23–28], although our results suggest that other acquisition as well as reconstruction methods can potentially be used for the same clinical purpose with each dose CT acquisition.

On the other hand, assessment of the effect of scanning method on the difference between CT numbers and the gold standard for the same reconstruction algorithm and tube current, wide-volume acquisition showed smaller differences than both of the helical acquisitions. In addition, 80-detector row helical acquisition resulted in slightly smaller differences than 64-detector row helical acquisition, and might be considered due to slightly smaller beam pit between 64-detector row helical acquisition (beam pitch 0.83) and 80-detector row helical acquisition (beam pitch 0.81). These findings were not surprising because wide-volume acquisition is a step-and-shoot acquisition. The previous studies have established that step-and-shoot acquisition is more useful for evaluating CT numbers than helical acquisition and a smaller beam pitch [19, 23–28]. Our results are, therefore, compatible with those previously reported. In addition, wide-volume acquisition as well as a smaller beam pitch for helical acquisition proved to be key issues for accurate evaluation of CT numbers of lung density measurements.

Assessment of the effect of the reconstruction algorithm on CT number assessment using the same acquisition method, the difference in CT numbers for FIRST was significantly smaller than that for FBP and AIDR 3D at each radiation dose. Moreover, the difference in CT numbers for AIDR 3D was significantly smaller than that for FBP at all tube currents except 400 mA. These findings also hinted at how significantly reduced image noise for FIRST or AIDR 3D methods might be affected to improve image quality and produce more accurate CT number assessment than with the FBP method on all other CT acquisitions [19, 23–28]. Moreover, it has been suggested that the FIRST method is capable of significantly reducing image noise and improving accuracy for quantitative evaluation with computer-aided volumetry more than is possible with the AIDR 3D method [28]. Our results, therefore, also suggest that FIRST is more useful than both the AIDR 3D and FBP method for quantitative lung CT number measurement with radiation dose reduction at 10 mA level for an ADCT examination.

Currently, QIBA is trying to standardize quantitative CT evaluation for lung density by 64-detector row helical acquisition with standard-radiation dose for all the vendors [18]. One phantom study by the QIBA lung density committee team, in an attempt to establish standard-dose CTs for four scanner manufacturers, reported that a mixed-effects model analysis using the lung foam that did not participate in the calibration as a test case showed that the 95% confidence intervals were − 862.0 HU to − 851.3 HU before standardization and − 859.0 HU to − 853.7 HU after standardization to 80 kVp. This study used three calibrated foam densities to establish an HU-electron density relationship for each machine protocol, and found that 95% confidence intervals for differences between CT numbers and gold standard ranged from − 6.1 HU to 4.6 HU before standardization, and from − 3.1 HU to 2.3 HU after standardization to 80 kVp [18]. Taking the above-mentioned results into consideration and utilizing a 320-detector row CT, all CT protocols using wide-volume and 80-detector row helical acquisition with the FIRST and AIDR 3D methods and by 64-detector row helical acquisition with the FIRST method were considered appropriate on the basis of smaller CT number variances. In addition, 64-detector row helical acquisition with the AIDR 3D method was also deemed to be capable of reducing the radiation dose to 50 mA level while maintaining smaller CT number variances. With the FBP method on the other hand, the ADCT could be used for 64-detector row helical acquisition at 400 mA, for 80-detector row helical acquisition at 400 mA, 100 mA, and 50 mA, and wide-volume acquisition at 400 mA, 100 mA, and 50 mA, while maintaining smaller CT number variance. Therefore, radiation dose reduction while maintaining accurate CT number assessment for chest CT is affected by not only scanning, but also reconstruction methods, and wide-volume acquisition with model-based iterative reconstruction (i.e., FIRST) methods would appear to be for use in routine clinical practice.

Our study has several limitations. First, although we directly evaluated measurement errors or variances in CT numbers, we did not standardize the findings to relative electron density or CT number at 80 kVp, similar to what was done in a previous study [18]. Therefore, our results were affected by differences in tube voltage as well as kernels on CT images reconstructed with the FBP and AIDR 3D methods. In addition, we applied FIRST and AIDR 3D and FBP methods. However, all the methods used in this study were provided by only one company, so that comparisons with methods provided by the other vendors could not be made. Moreover, reconstruction time for the FIRST method was 10 min, slightly longer than others. Therefore, further studies are warranted to assess the actual potentials of the newly developed model-based iterative reconstruction methods. Second, we used the FBP, AIDR 3D, and FIRST methods for thin-section CT image reconstruction. In addition, we used soft-tissue kernels, and did not evaluate lung kernels from the point of view of use of quantitative CT evaluation for COPD assessment. In addition, we applied AIDR 3D and FIRST methods at standard levels, and did not assess them at other levels. Therefore, further investigations were also recommended. Third, although mean CT number had significant difference between all CT protocols by 64- and 80-detector row CTs and 10 mA-CT by wide-volume scan and gold standard, among different

Table 3 Differences between actual and measured CT numbers using three different acquisition methods and the same tube current and reconstruction method

CT protocol	Reconstruction method	Acquisition method	Difference between actual and measured CT numbers (HU) (Mean ± standard deviation)
400 mA-CT	FBP	64-Detector row helical acquisition	−5.3 ± 0.2
		80-Detector row helical acquisition	−2.8 ± 0.2*
		Wide-volume acquisition	−1.8 ± 0.1*,**
	AIDR 3D	64-Detector row helical acquisition	−5.3 ± 0.2
		80-Detector row helical acquisition	−2.9 ± 0.1*
		Wide-volume acquisition	−1.8 ± 0.1*,**
	FIRST	64-Detector row helical acquisition	−2.0 ± 0.2
		80-Detector row helical scan	−0.5 ± 0.1*
		Wide-volume acquisition	−0.2 ± 0.1*,**
100 mA-CT	FBP	64-Detector row helical acquisition	−5.9 ± 0.2
		80-Detector row helical acquisition	−3.6 ± 0.1*
		Wide-volume acquisition	−2.4 ± 0.2*,**
	AIDR 3D	64-Detector row helical acquisition	−5.5 ± 0.2
		80-Detector row helical acquisition	−3.2 ± 0.1*
		Wide-volume acquisition	−2.0 ± 0.2*,**
	FIRST	64-Detector row helical acquisition	−2.2 ± 0.4
		80-Detector row helical acquisition	−0.8 ± 0.2*
		Wide-volume acquisition	0.2 ± 0.4*,**
50 mA-CT	FBP	64-Detector row helical acquisition	−6.4 ± 0.3
		80-Detector row helical acquisition	−4.3 ± 0.2*
		Wide-volume acquisition	−2.9 ± 0.3*,**
	AIDR 3D	64-Detector row helical acquisition	−5.4 ± 0.2
		80-Detector row helical acquisition	−3.3 ± 0.1*
		Wide-volume acquisition	−2.0 ± 0.3*,**
	FIRST	64-Detector row helical acquisition	−2.5 ± 0.4
		80-Detector row helical acquisition	−0.8 ± 0.4*
		Wide-volume acquisition	0.3 ± 0.4*,**
20 mA-CT	FBP	64-Detector row helical acquisition	−8.8 ± 0.1
		80-Detector row helical acquisition	−6.4 ± 0.3*
		Wide-volume acquisition	−5.5 ± 0.4*, **
	AIDR 3D	64-Detector row helical acquisition	−5.7 ± 0.1
		80-Detector row helical acquisition	−3.4 ± 0.2*
		Wide-volume acquisition	−2.4 ± 0.3*,**
	FIRST	64-Detector row helical acquisition	−3.1 ± 0.1
		80-Detector row helical acquisition	−1.0 ± 0.4*
		Wide-volume acquisition	0.4 ± 0.4*,**
10 mA-CT	FBP	64-Detector row helical acquisition	−14.0 ± 0.4
		80-Detector row helical acquisition	−12.6 ± 0.4*
		Wide-volume acquisition	−5.5 ± 0.4*,**
	AIDR 3D	64-Detector row helical acquisition	−6.3 ± 0.4
		80-Detector row helical acquisition	−4.2 ± 0.4*
		Wide-volume acquisition	−3.0 ± 0.4*,**
	FIRST	64-Detector row helical acquisition	−3.6 ± 0.4
		80-Detector row helical acquisition	−1.7 ± 0.4*
		Wide-volume acquisition	−0.5 ± 0.4*,**

FBP filtered back projection, *AIDR 3D* adaptive iterative dose reduction using 3D processing, *FIRST* forward projected model-based iterative reconstruction

*Significant difference with 64-detector row helical acquisition ($p < 0.0001$)

**Significant difference with 80-detector row helical acquisition ($p < 0.0001$)

Table 4 Differences between actual and measured CT number using three reconstruction methods and the same acquisition method and tube current

Acquisition method	CT protocol	Reconstruction method	Difference between actual and measured CT number (HU) (mean ± standard deviation)
64-detector row helical acquisition	400 mA-CT	FBP	−5.3 ± 0.2
		AIDR 3D	−5.3 ± 0.2
		FIRST	−2.0 ± 0.2*,**
	100 mA-CT	FBP	−5.9 ± 0.2
		AIDR 3D	−5.5 ± 0.2*
		FIRST	−2.2 ± 0.4*,**
	50 mA-CT	FBP	−6.4 ± 0.3
		AIDR 3D	−5.4 ± 0.2*
		FIRST	−2.5 ± 0.4*,**
	20 mA-CT	FBP	−8.8 ± 0.1
		AIDR 3D	−5.7 ± 0.1*
		FIRST	−3.1 ± 0.1*,**
	10 mA-CT	FBP	−14.0 ± 0.4
		AIDR 3D	−6.3 ± 0.4*
		FIRST	−3.6 ± 0.4*,**
80-detector row helical acquisition	400 mA-CT	FBP	−2.8 ± 0.2
		AIDR 3D	−2.9 ± 0.1
		FIRST	−0.5 ± 0.1*,**
	100 mA-CT	FBP	−3.6 ± 0.1
		AIDR 3D	−3.2 ± 0.1*
		FIRST	−0.8 ± 0.2*,**
	50 mA-CT	FBP	−4.3 ± 0.2
		AIDR 3D	−3.3 ± 0.1*
		FIRST	−0.8 ± 0.4*,**
	20 mA-CT	FBP	−6.4 ± 0.3
		AIDR 3D	−3.4 ± 0.2*
		FIRST	−1.0 ± 0.4*,**
	10 mA-CT	FBP	−12.6 ± 0.4
		AIDR 3D	−4.2 ± 0.4*
		FIRST	−1.7 ± 0.4*,**
Wide-volume acquisition	400 mA-CT	FBP	−1.8 ± 0.1
		AIDR 3D	−1.8 ± 0.1
		FIRST	−0.2 ± 0.1*,**
	100 mA-CT	FBP	−2.4 ± 0.2
		AIDR 3D	−2.0 ± 0.2*
		FIRST	0.2 ± 0.4*,**
	50 mA-CT	FBP	−2.9 ± 0.3
		AIDR 3D	−2.0 ± 0.3*
		FIRST	0.3 ± 0.4*,**
	20 mA-CT	FBP	−5.5 ± 0.4
		AIDR 3D	−2.4 ± 0.3*
		FIRST	0.4 ± 0.4*,**
	10 mA-CT	FBP	−5.5 ± 0.4
		AIDR 3D	−3.0 ± 0.4*
		FIRST	−0.5 ± 0.4*,**

FBP filtered back projection, *AIDR 3D* adaptive iterative dose reduction using 3D processing, *FIRST* forward projected model-based iterative reconstruction

*Significant difference with FBP method ($p < 0.0001$)

**Significant difference with AIDR 3D method ($p < 0.0001$)

Table 5 Limits of agreement between actual and measured CT number in lung density phantom for all CT protocols

CT protocol	Reconstruction method	Acquisition method	Limits of agreement between actual and measured CT numbers in lung density phantom (Mean ± 1.96 × standard deviation [HU])
400 mA-CT	FBP	64-Detector row helical acquisition	−5.3 ± 0.4
		80-Detector row helical acquisition	−2.8 ± 0.4
		Wide-volume acquisition	−1.8 ± 0.2
	AIDR 3D	64-Detector row helical acquisition	−5.3 ± 0.4
		80-Detector row helical acquisition	−2.9 ± 0.2
		Wide-volume acquisition	−1.8 ± 0.2
	FIRST	64-Detector row helical acquisition	−2.0 ± 0.4
		80-Detector row helical acquisition	−0.5 ± 0.2
		Wide-volume acquisition	−0.2 ± 0.2
100 mA-CT	FBP	64-Detector row helical acquisition	−5.9 ± 0.4
		80-Detector row helical acquisition	−3.6 ± 0.2
		Wide-volume acquisition	−2.4 ± 0.4
	AIDR 3D	64-Detector row helical acquisition	−5.5 ± 0.4
		80-Detector row helical acquisition	−3.2 ± 0.2
		Wide-volume acquisition	−2.0 ± 0.4
	FIRST	64-Detector row helical acquisition	−2.2 ± 0.8
		80-Detector row helical acquisition	−0.8 ± 0.4
		Wide-volume acquisition	0.2 ± 0.8
50 mA-CT	FBP	64-Detector row helical acquisition	−6.4 ± 0.6
		80-Detector row helical acquisition	−4.3 ± 0.4
		Wide-volume acquisition	−2.9 ± 0.6
	AIDR 3D	64-Detector row helical acquisition	−5.4 ± 0.4
		80-Detector row helical acquisition	−3.3 ± 0.2
		Wide-volume acquisition	−2.0 ± 0.6
	FIRST	64-Detector row helical acquisition	−2.5 ± 0.8
		80-Detector row helical acquisition	−0.8 ± 0.8
		Wide-volume acquisition	0.3 ± 1.2
20 mA-CT	FBP	64-Detector row helical acquisition	−8.8 ± 0.2
		80-Detector row helical acquisition	−6.4 ± 0.6
		Wide-volume acquisition	−5.5 ± 0.8
	AIDR 3D	64-Detector row helical acquisition	−5.7 ± 0.2
		80-Detector row helical acquisition	−3.4 ± 0.4
		Wide-volume acquisition	−2.4 ± 0.6
	FIRST	64-Detector row helical acquisition	−3.1 ± 0.2
		80-Detector row helical acquisition	−1.0 ± 0.8
		Wide-volume acquisition	0.4 ± 0.8
10 mA-CT	FBP	64-Detector row helical acquisition	−14.0 ± 0.8
		80-Detector row helical acquisition	−12.6 ± 0.8
		Wide-volume acquisition	−5.5 ± 0.8
	AIDR 3D	64-Detector row helical acquisition	−6.3 ± 0.8
		80-Detector row helical acquisition	−4.2 ± 0.8
		Wide-volume acquisition	−3.0 ± 0.8
	FIRST	64-Detector row helical acquisition	−3.6 ± 0.8
		80-Detector row helical acquisition	−1.7 ± 0.8
		Wide-volume acquisition	−0.5 ± 0.8

FBP filtered back projection, *AIDR 3D* adaptive iterative dose reduction using 3D processing, *FIRST* forward projected model-based iterative reconstruction

acquisition methods at each tube current and among different reconstruction methods at each tube current, these differences were not determined as clinically significant in this study. In addition, the uniformity difference within scan volume was not evaluated between wide-volume scan and both detector row helical scans. Therefore, further investigation might be warranted. Fourth, although we evaluated the effect of scanning method and reconstruction method for radiation dose reduction on quantitatively assessed CT numbers, we did not evaluate the effect on RA_{950} and PD15 measurements in an in vivo study. In addition, we had not evaluated the other indexes such as the RA960 suggested by Madani et al. [7] and 15th percentile point of the density histogram (i.e., P15), which were used in a few studies including COPD Gene study [8, 29, 30], in this study, because we followed previous QIBA studies [15–18]. We are, therefore, considering additional assessments of radiation dose reduction as a result of combining these techniques as well as other indexes and to determine the clinical significance of such techniques for quantitatively assessed CT evaluation of COPD. Fifth, we evaluated one single model of CT (i.e., Aquilion ONE) and did not directly compare the other scanners in this study. In addition, we only apply AIDR 3D and FIRST as hybrid-type and model-based IR methods and did not assess the other IR techniques and CTs provided by the other vendors. We, therefore, consider to directly compare Aquilion ONE with the other scanners provided by not only Canon Medical, but also other vendors, and AIDR 3D or FIRST with other IR techniques provided by other CT vendors in near future.

In conclusion, scan and reconstruction methods used for ADCT had a significant effect on radiation dose reduction and accuracy of CT lung density measurements in a QIBA recommended phantom study. In addition, the use of the newly developed FIRST and AIDR 3D methods for 80-detector row helical and wide-volume acquisitions showed that radiation dose can be reduced to a level of less than 4% (i.e., 10 mA) of that for the standard dose recommended by the QIBA CT lung density committee team while maintaining sufficient accuracy of CT number measurements.

Funding This work is "Original Research" and Dr. Ohno had a research grant from the Canon Medical Systems Corporation. Ms. Fujisawa, Mr. Fujii and Mr. Sugihara are employees of Canon Medical Systems Corporation.

References

1. Dirksen A, Friis M, Olesen KP, Skovgaard LT, Sørensen K. Progress of emphysema in severe alpha 1-antitrypsin deficiency as assessed by annual CT. Acta Radiol. 1997;38:826–32.
2. Madani A, Zanen J, de Maertelaer V, Gevenois PA. Pulmonary emphysema: objective quantification at multi-detector row CT-comparison with macroscopic and microscopic morphometry. Radiology. 2006;238:1036–43.
3. Madani A, De Maertelaer V, Zanen J, Gevenois PA. Pulmonary emphysema: radiation dose and section thickness at multidetector CT quantification-comparison with macroscopic and microscopic morphometry. Radiology. 2007;243:250–7.
4. Madani A, Van Muylem A, de Maertelaer V, Zanen J, Gevenois PA. Pulmonary emphysema: size distribution of emphysematous spaces on multidetector CT images-comparison with macroscopic and microscopic morphometry. Radiology. 2008;248:1036–41.
5. Stoel BC, Putter H, Bakker ME, et al. Volume correction in computed tomography densitometry for follow-up studies on pulmonary emphysema. Proc Am Thorac Soc. 2008;5:919–24.
6. Coxson HO. Sources of variation in quantitative computed tomography of the lung. J Thorac Imaging. 2013;28:272–9.
7. Shaker SB, Dirksen A, Laursen LC, Skovgaard LT, Holstein-Rathlou NH. Volume adjustment of lung density by computed tomography scans in patients with emphysema. Acta Radiol. 2004;45:417–23.
8. Iyer KS, Grout RW, Zamba GK, Hoffman EA. Repeatability and sample size assessment associated with computed tomography-based lung density metrics. Chronic Obstr Pulm Dis. 2014;1:97–104.
9. Keller BM, Reeves AP, Henschke CI, Yankelevitz DF. Multivariate compensation of quantitative pulmonary emphysema metric variation from low-dose, whole-lung CT scans. AJR Am J Roentgenol. 2011;197:W495–502.
10. Park SJ, Lee CH, Goo JM, Heo CY, Kim JH. Inter-scan repeatability of CT-based lung densitometry in the surveillance of emphysema in a lung cancer screening setting. Eur J Radiol. 2012;81:e554–60.
11. Gietema HA, Schilham AM, van Ginneken B, van Klaveren RJ, Lammers JW, Prokop M. Monitoring of smoking-induced emphysema with CT in a lung cancer screening setting: detection of real increase in extent of emphysema. Radiology. 2007;244:890–7.
12. Chong D, Brown MS, Kim HJ, et al. Reproducibility of volume and densitometric measures of emphysema on repeat computed tomography with an interval of 1 week. Eur Radiol. 2012;22:287–94.
13. Hochhegger B, Irion KL, Marchiori E, Moreira JS. Reconstruction algorithms and their influence in emphysema CT measurements. Acad Radiol. 2010;17:674.
14. Diciotti S, Sverzellati N, Kauczor HU, et al. Defining the intra-subject variability of whole-lung CT densitometry in two lung cancer screening trials. Acad Radiol. 2011;18:1403–11.
15. QIBA (2017) Lung density profile under development and will appear. https://www.rsna.org/QIBA-Profiles-in-Development/.
16. QIBA (2017) Lung density COPDGene 2 phantom design, CTP698 and CCT162 COPDGene® lung phantom II. http://www.phantomlab.com/other-catphans.
17. Sieren JP, Newell JD, Judy PF, et al. Reference standard and statistical model for intersite and temporal comparisons of CT attenuation in a multicenter quantitative lung study. Med Phys. 2012;39:5757–67.
18. Chen-Mayer HH, Fuld MK, Hoppel B, et al. Standardizing CT lung density measure across scanner manufacturers. Med Phys. 2017;44:974–85.
19. Ohno Y, Takenaka D, Kanda T, et al. Adaptive iterative dose reduction using 3D processing for reduced- and low-dose pulmonary CT: comparison with standard-dose CT for image noise reduction and radiological findings. AJR Am J Roentgenol. 2012;199:W477–85.
20. Bland JM, Altman DG. Measurement error. BMJ. 1996;312:1654.

21. Bland JM, Altman DG. Statistical methods for assessing agreement between two methods of clinical measurement. Lancet. 1986;1:307–10.
22. Bland JM, Altman DG. Agreed statistics: measurement method comparison. Anesthesiology. 2012;116:182–5.
23. Nishio M, Matsumoto S, Ohno Y, et al. Emphysema quantification by low-dose CT: potential impact of adaptive iterative dose reduction using 3D processing. AJR Am J Roentgenol. 2012;199:595–601.
24. Nishio M, Matsumoto S, Seki S, et al. Emphysema quantification on low-dose CT using percentage of low-attenuation volume and size distribution of low-attenuation lung regions: effects of adaptive iterative dose reduction using 3D processing. Eur J Radiol. 2014;83:2268–76.
25. Nagatani Y, Takahashi M, Murata K, Investigators of ACTIve Study Group, et al. Lung nodule detection performance in five observers on computed tomography (CT) with adaptive iterative dose reduction using three-dimensional processing (AIDR 3D) in a Japanese multicenter study: comparison between ultra-low-dose CT and low-dose CT by receiver-operating characteristic analysis. Eur J Radiol. 2015;84:1401–12.
26. Ohno Y, Koyama H, Fujisawa Y, et al. Hybrid Type iterative reconstruction method vs. filter back projection method: capability for radiation dose reduction and perfusion assessment on dynamic first-pass contrast-enhanced perfusion chest area-detector CT. Eur J Radiol. 2016;85:164–75.
27. Nishio M, Koyama H, Ohno Y, et al. Emphysema quantification using ultralow-dose CT with iterative reconstruction and filtered back projection. AJR Am J Roentgenol. 2016;206:1184–92.
28. Ohno Y, Yaguchi A, Okazaki T, et al. Comparative evaluation of newly developed model-based and commercially available hybrid-type iterative reconstruction methods and filter back projection method in terms of accuracy of computer-aided volumetry (CADv) for low-dose CT protocols in phantom study. Eur J Radiol. 2016;85:1375–82.
29. Kim V, Davey A, Comellas AP, COPDGene® Investigators, et al. Clinical and computed tomographic predictors of chronic bronchitis in COPD: a cross sectional analysis of the COPDGene study. Respir Res. 2014;15:52.
30. Oelsner EC, Smith BM, Hoffman EA, et al. Prognostic significance of large airway dimensions on computed tomography in the general population. The multi-ethnic study of atherosclerosis (MESA) lung study. Ann Am Thorac Soc. 2018;15:718–27.